Asian Journal of Chemistry; Vol. 37, No. 8 (2025), 2022-2030

ASIAN JOURNAL OF CHEMISTRY

https://doi.org/10.14233/ajchem.2025.34100

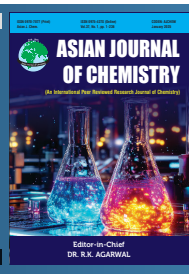

Batch Adsorptive Removal Studies of Chromium(VI) using Cellulose-based Crosslinked Hydrogel

GOVINDASWAMY PERIYANNAN and SRINIVASAN LATHA*

Department of Chemistry, Vellore Institute of Technology, Vellore-632014, India

*Corresponding author: E-mail: srinivasan.latha@vit.ac.in

Received: 22 May 2025; *Accepted*: 18 July 2025; *Published online*: 31 July 2025; AJC-22081

This study reports the removal of hexavalent chromium [Cr(VI)] using a novel cellulose-based crosslinked hydrogel synthesized from chitosan oligosaccharide (COS), nanocrystalline cellulose (NCC), acrylamide (AM) and N.N′-methyl *bis*-acrylamide (MBA) as crosslinker. The hydrogel was characterized by FTIR, XRD, SEM, EDAX, particle size analysis and zeta potential. Batch adsorption experiments evaluated the effects of pH, contact time, initial Cr(VI) concentration and adsorbent dosage. Results showed that the COS-NCC-*g*-AM/MBA hydrogel exhibited high adsorption capacity and removal efficiency under optimal conditions. The adsorption was strongly influenced by operational parameters. Overall, the composite presents a sustainable, low-cost and efficient solution for removal of Cr(VI) from wastewater, demonstrating significant potential for water purification and environmental remediation applications.

Keywords: Chitosan oligosaccharide, Cellulose-based hydrogel, Chromium ions, Adsorption, Batch studies.

INTRODUCTION

The removal of hazardous heavy metals from industrial wastewater and drinking water has become a critical issue in recent years, requiring the development of cost-effective, safe and efficient methods. Even in trace amounts, heavy metals are highly toxic to living organisms and do not easily degrade in nature [1]. Chromium and its components are widely used in industries such as tanning, glass ceramics, chrome plating, photography, wood preservation and in the production of fungicides, pigments, catalysts and chrome alloys [2]. Methods commonly employed to remove heavy metals from water include membrane filtration, precipitation, coagulation, flocculation, electrochemical treatment, adsorption and nanotechnology based techniques [3,4]. However, the removal of specific chromium species can be challenging due to their resistance to many conventional techniques. Furthermore, these methods are often expensive, produce secondary pollutants, consume a lot of energy, how low chromium removal efficiency and involve lengthy processing times, along with limited adsorbent regeneration [5,6].

Adsorption, a physico-chemical process, is widely favoured over other techniques due to its simplicity, low cost, recyclability and environmental friendly nature [7]. Various biopolymer based adsorbents have been investigated over time for removing heavy metal ions from aqueous solutions [8,9]. Ideal adsorbents are expected to be cost-effective with high selectivity, minimum dosage requirements and substantial adsorption capacity. Furthermore, they should achieve rapid binding kinetics, reach equilibrium within a reasonable time, support easy regeneration and improve adsorption efficiency without harming the environment. Biopolymer-based hydrogels, which are biodegradable, hydrophilic and eco-friendly, have garnered attention for their enhanced performance and specificity [10]. Hydrogels made from materials like chitosan, lignin, gelatin and gums are often used in adsorbent synthesis [11].

Currently, most commercially available superabsorbent products such as baby diapers are made from petroleum based vinyl monomers, making them poorly degradable and environmental unfriendly [12]. Growing concerns for environmental preservation and green chemistry have led to increasing interest in biodegradable materials [13]. Consequently, renewable and biodegradable polymers are becoming more attractive due to their abundant availability, low production costs and biodegradability. Natural polysaccharide-based hydrogels, which are three-dimensional networks of hydrophilic and hydrophobic polymers are capable of absorbing large amounts of water and show potential as effective adsorbents [14]. In present study, chitosan oligosaccharide (COS) was blended with nanocellulose,

grafted with acrylamide and crosslinked with methylene *bis*-acrylamide (MBA) to prepare an interpenetrating network (IPN) hydrogel. The material was then characterized and analyzed for its ability to remove chromium(VI) from water through batch adsorption processes.

EXPERIMENTAL

Key materials used in this study include chitosan oligosaccharide (COS) obtained from India Sea Foods, Kerala, India. Ceric ammonium nitrate (CAN) was purchased from Thomas Baker Pvt Ltd. Acetic acid and cellulose were supplied by S.D. Fine-Chem Ltd. Mumbai, India and potassium dichromate and methylene *bis*-acrylamide (MBA) was sourced from Sigma-Aldrich, USA. Commercial-grade sodium hydroxide was provided by Central Drug House Pvt Ltd., India. All other chemicals were conducted using analytical-grade reagents.

Preparation of nanocrystalline cellulose (NCC): Cellulose (5 g) were mixed with 50 mL of sulfuric acid (1:2 ratio) and agitated at 45 ºC for 1 h. Afterward, 100 mL of cold water was added to halt the acid hydrolysis process and the obtained NCC was separated by centrifugation. The material was washed repeatedly until neutral pH was achieved.

Preparation of COS-NCC hydrogel: Chitosan oligosaccharide (COS, 1 g) dissolved in 50 mL of deionized water was added to the NCC suspension at 50 ºC to form a homogenous mixture. Ascorbic acid (7.2 g) and the initiator CAN (0.072 g) were introduced into the mixture, followed by the addition to the crosslinker MBA (0.0036 g). Then, the solution was mixed thoroughly for 1 h, then poured into a mold to form the hydrogel (Fig. 1).

Fig. 1. Images of COS-NCC-AM/MBA hydrogel

Characterization: The FTIR spectra (Shimadzu IR Affinity-1S spectrometer) were obtained in the range of 4000-400 cm^{-1} using KBr pellet. The crystallinity of the developed samples was determined using a powder X-ray diffractometer (XRD-Shimadzu XD - DI) equipped with a Ni-filtered Cu*K*α X-ray radiation source. The surface morphology of the samples was analyzed using scanning electron microscope (SEM) for high-resolution surface imaging. The JEOL Model JSM- 6390LY was employed at a magnification of X250 and surface imaging was conducted at an accelerating voltage of 20 kV.

Particle size and zeta potential measurement: The specific surface area, pore volume and pore size of the hydrogel were measured using N_2 adsorption/desorption isotherms, with data collected through a NOVA-2200e instrument. A Quanta chrome surface area analyzer was used for the analysis and the Brunauer-Emmet-Teller (BET) method was applied for the calculations.

Adsorption studies: The removal of Cr(VI) from standard solutions was assessed using the synthesized COS-NCC-*g*-AM/MBA hydrogel *via* the batch adsorption method. An aqueous solution was prepared by dissolving 0.283 g of $K_2Cr_2O_7$ in 1000 mL of deionized water. The adsorption kinetics of Cr(VI) were examined by shaking 1 g of hydrogel with 100 mL of chromium(VI) stock solution. Adjustments to the initial pH were made using 2 N HCl and 2 N NaOH as needed. The pH-modified solution was agitated in an orbital shaker at 200 rpm for 60 min at 28 ºC, which was determined as the optimal contact time. The experiment followed the prescribed protocol, with the reaction mixture being filtered using Whatman filter paper after 1 h of agitation. The Cr(VI) concentration in the filtrate was determined using atomic absorption spectroscopy (AAS). Similar procedures were used to investigate the effects of initial chromium concentration, adsorbent dosage, pH and contact time. Upon completion of the adsorption process, the percentage removal (%) and adsorption capacity (mg/g) were calculated using the following equations:

$$\text{Removal } (\%) = \frac{\text{Initial metal conc.} - \text{Final metal conc.}}{\text{Initial concentration}} \times 100 \quad (1)$$

$$\text{Adsorption capacity } (q_e) = \frac{C_o - C_e \times V}{m} \quad (2)$$

where m = weight of the dry adsorbent (g), V = volume of the solution (L), C_o = initial metal ion concentration, C_e = final metal ion concentration.

Adsorption isotherms: To further explore the adsorption mechanism, the isotherm for Cr(VI) adsorption on the hydrogel was studied. The Langmuir and Freundlich isotherms, two commonly used models to interpret adsorption behaviour, were applied in the analysis. The mathematical expressions for the Langmuir and Freundlich models are given in eqns. 3 and 4, respectively.

$$\frac{C_e}{q_e} = \frac{1}{K_L q_m} + \frac{C_e}{q_m} \quad (3)$$

$$\frac{C_{eq}}{C_{ads}} = C_{eq} C_{max} + 1 K_L C_{max} = K_L b$$

where C_{eq} = equilibrium concentration of the remaining heavy metal ion in solution (mg/g), C_{ads} = quantity of metal ion adsorbed (mg/g), C_{max} = adsorption capacity (mg/g), b = Langmuir constant (dm^3/mg), K_L = Langmuir constant (dm^3/mg).

The equilibrium adsorption data was plotted as C_{eq} *versus* C_{eq}/C_{ads} to calculate the R^2 value, which measures how well the experimental data fits the mathematical isotherm model. The R_L values are used to predict the favourability of the biosorption system. When $R_L < 1$, the process is favourable; $R_L > 1$ indicates an unfavourable process; $R_L = 1$ suggests a linear relationship and $R_L = 0$ points to an irreversible process.

The Freundlich isotherm model, in its linear form is represented by the following equation:

$$\log q_e = \log K_f + \left(\frac{1}{n}\right)\log C_e \quad (4)$$

where 1/n = dimensionless Freundlich exponent heterogeneity coefficient, C_e = Cr(VI) ion concentration at equilibrium in an aqueous phase, q_e = amount adsorbed per unit weight of adsorbent at equilibrium, K_F = Freundlich constant related to adsorption capacity (mg/g).

A plot of log q_e *versus* log C_e results in an intercept of log K_F and a slope of 1/n.

Kinetics of adsorption: Adsorption kinetics play a crucial role in determining the efficiency of the adsorption process. The adsorption kinetic data were analyzed using pseudo-first-order (PFO), pseudo-second-order (PSO) and intraparticle diffusion (IPD) models to gain insights into the adsorption mechanism. The corresponding equations for these models are given below:

$$\log(q_e - q_t) = \log q_e - \frac{k_1 t}{2.303} \quad (5)$$

$$\frac{t}{q_t} = \frac{1}{k_2 q^2 e} + \frac{t}{q_e} \quad (6)$$

here q_e (mg/g) represents the hydrogel's adsorption capacity at time t. The equilibrium adsorption capacity of the hydrogel was calculated using both pseudo-first-order (PFO), pseudo-second-order (PSO) kinetic models and is indicated by q_e (mg/g). the adsorption rate constants for the PFO and PSO models are denoted by K_1 (min^{-1}) and K_2 (g/mg. min), respectively.

The intraparticle diffusion model (IPD) is described by the following equation:

$$q_t = K_{id}^{½} + C \quad (7)$$

In this equation, K_{id} and C represent the intraparticle diffusion rate and constant, respectively.

Desorption: To facilitate the desorption of metal ions bound to the adsorbent, 0.1 M HCl and 0.1 M EDTA were added. The metal- loaded adsorbent was individually treated with 100 mL of 0.1 M HCl and 0.1M EDTA. Aliquots were taken at individuals of 1, 2, 3, 4 and 5 h for analysis. The desorption ratio was calculated using the amount of metal ions adsorbed and the final concentration of metal ions in the desorption medium:

$$\text{Desorption ratio} = \frac{\text{Amount of metal ions desorbed}}{\text{Amount of metal ions adsorbed}} \times 100$$

RESULTS AND DISCUSSION

Hydrogels are effective adsorbents for heavy metal removal due to their polymeric networks containing diverse functional groups that bind metal ions. The adsorption mechanism in hydrogels is governed by both chemical and physical interactions, including hydrophobic, coordination, electrostatic contact and ion-exchange processes [15]. The obtained hydrogel in this study has a fluffy, porous structure, even after standard drying, which enhances its potential for heavy metal adsorption. The functional groups present in COS, nanocellulose and polyacrylamide, crosslinked with MBA are anticipated to provide a high surface area, making them highly suitable for metal ion adsorption. The COS-CL-*g*-AM/MBA hydrogel underwent characterization *via* multiple techniques before being evaluated for its chromium(VI) adsorption capabilities.

Swelling studies: The hydrogel maintained its insolubility in water for oven 10 h. The weight of the swollen hydrogel was recorded every 30 min, as shown in Fig. 2. The swelling ratio of 10.62 g/g demonstrates its excellent hydrophilicity of hydrogel. A highly swollen hydrogel facilitates the diffusion of heavy metal ions, enabling their attachment to adsorption sites within the hydrogel material [16]. This characteristic supports its suitability for metal adsorption.

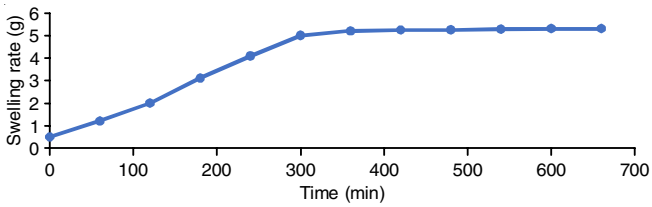

Fig. 2. Swelling analysis of COS-CL-*g*-AM/MBA hydrogel

FTIR studies: The surface functional groups of the modified COS-based hydrogel were identified through FTIR analysis. In Fig. 3, bands at 3339 cm^{-1} and 3179 cm^{-1} are associated with the symmetric and asymmetric stretching vibrations of the N-H group in the primary amide, as well as both intramolecular hydrogen bonding, as reported by Linares *et al.* [17]. The peaks at 3038 cm^{-1} and 2018 cm^{-1} correspond to the C-H stretching vibrations [18]. Mahato *et al.* [19] observed that the carbonyl group of COS is represented by peak at 1635 cm^{-1}, while the C=O stretching vibrations of amide in the sample by the peak at 1665 cm^{-1} [20]. This blue shift indicates successful hydrogel formation [19]. The peak at 1609 cm^{-1} is attributed to N-H bending vibrations [21], as the C-N stretching vibrations are marked by the wavenumber 1424 cm^{-1} [22]. The peak at 1350 cm^{-1} is ascribed to the stretching vibrations of the C-O group [23] and the peak at 1135 cm^{-1} reflects the vibration of the C-O group in primary and secondary alcohols [24]. Finally, the peaks at 986.07 and 1051 cm^{-1} correspond to the C-O-C glycosidic linkages [25,26]. While comparing the FTIR spectra of COS and the hydrogel, the appearance of new peaks and shifts in existing peaks further confirms the successful synthesis of the hydrogel.

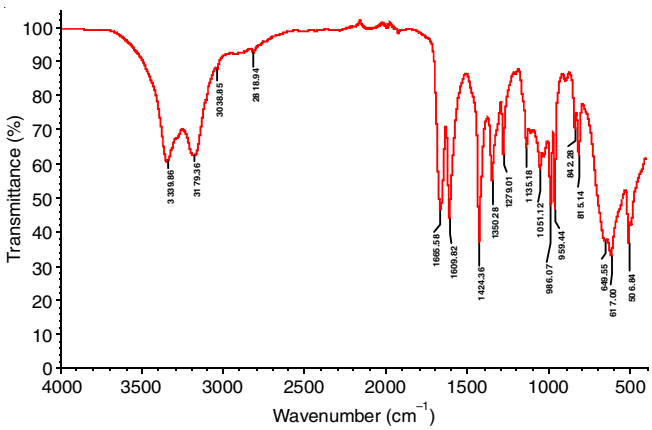

Fig. 3. FTIR spectrum of COS-CL-*g*-AM/MBA hydrogel

BET analysis: The total pore volume, BET surface area and average pore size of COS and COS-CL-*g*-AM/MBA are presented in Table-1. Following the modification of COS trough blending with nanocellulose, grafting and crosslinking with acrylamide and methylene *bis*-acrylamide to form the hydrogel, the BET surface area of the support increased from 90.97 to 245.21 $m^2 g^{-1}$. This increase occurs because, during the modification process, both the surface and internal regions of COS become more porous due to grafting with functional acrylamide and crosslinking into an interpenetrating network by MBA. This process reduces pore volume and size, while significantly enhancing the active surface area. Therefore, the modification successfully improved the surface properties of COS [27].

TABLE-1
SURFACE PROPERTIES OF COS AND COS-CL-*g*-AM/MBA

Sample	Surface area S_{BET} (m^2/g)	Pore volume V_{total} (cc/g)	Pore size Dv (nm)
COS	90.97	1.1	9.3
COS-CL-*g*-AM/MBA	245.21	0.62	1.51

XRD studies: The X-ray diffractograms of COS and the synthesized hydrogel are shown in Fig. 4 indicates that COS has a semicrystalline structure. Both COS and COS-CL-*g*-AM/MBA exhibit semicrystalline characteristics, containing both crystalline and amorphous regions. Peaks are observed at 2θ values of 10º and 20º for COS and at 11.7º, 18º, 19.1º, 20.3º, 22.3º, 23.6º and 28.2º for COS-CL-*g*-AM/MBA (Table-2). As per the literature, chitosan oligosaccharide shows characteristic peaks at 2θ values of 10º and 20º, which correspond to its two crystal forms, I and II [28]. Comparing the XRD patterns of the resultant hydrogel and chitosan oligosaccharides reveals a decrease in the intensity of the peak at 13º and a shift of the peak at 22º to 22.7º, indicating a transformation in the crystal structure. The percentage crystallinity, calculated using the method as described by Nara & Komiya [29], decreased from 23.4% for COS to 8.7% for hydrogel. This reduction in the crystallinity suggests an increase in the amorphous nature of the material, making it more favourable for adsorption [8].

TABLE-2
X-RAY DIFFRACTION DATA

Sample	2θ	Crystallinity (%)
COS	10, 20	23.4
COS-CL-*g*-AM/MBA	11.7, 18, 19.1, 20.3, 22.7, 23.6, 28.2	8.7

Thermal studies: The DSC thermogram of COS-CL-*g*-AM/MBA hydrogel reveals an endothermic peak at about 85 ºC, Fig. 5 indicates the presence of one crystalline form and the evaporation of water molecules. The appearance of a single glass transtion temperature (T_g) at 150 ºC indicates complete mixing and maximum COS interaction with other polymers *via* the highest number of hydrogen bonds, which results in high thermal stability. The superior thermal stability is further demonstrated by the thermogram, which reveals that it did not decompose upto 300 ºC.

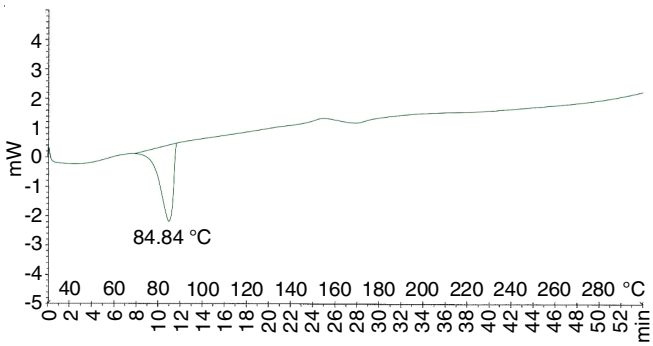

Fig. 5. DSC thermogram of COS-CL-*g*-AM/MBA hydrogel

SEM studies: The SEM images (Fig. 6) revealed a coarse and irregular surface topography. When compared with the SEM image of pure COS [30], it is evident that the hydrogel has developed concavities. The hydrogel features voids and pores, which are advantageous for adsorption. Tiny pores and holes are visible on the surface of the SEM images [31]. The roughness of the pore walls provides additional contact points for metal ions by allowing heavy metal chromium ions to pass through water, which acts as a transport medium, from the metal solutions to the adsorbent network through the abundant pore

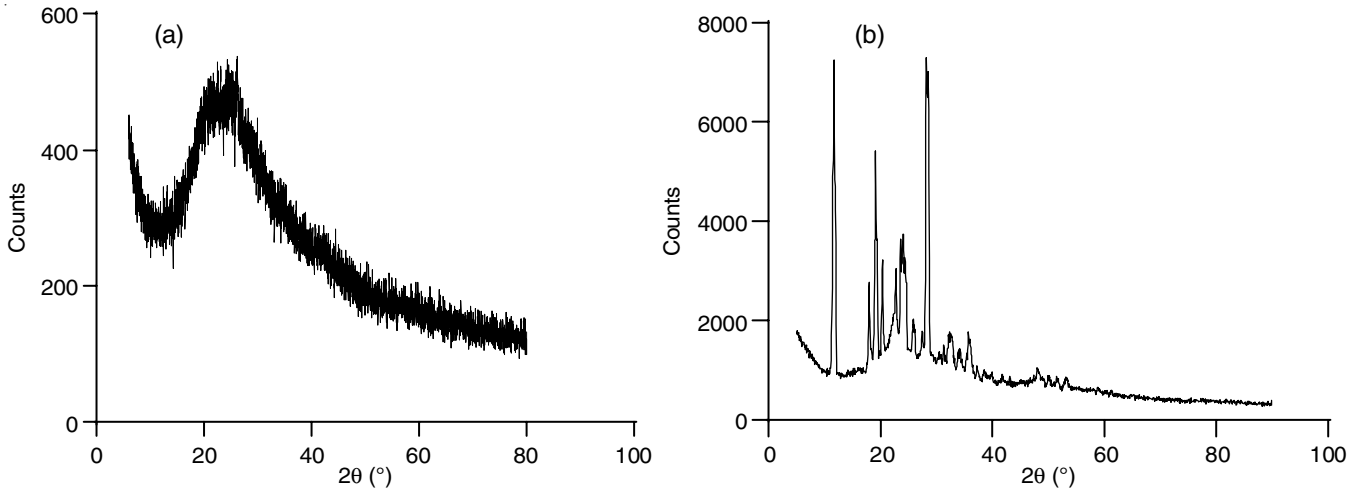

Fig. 4. XRD patterns of (a) COS and (b) COS-CL-*g*-AM/MBA

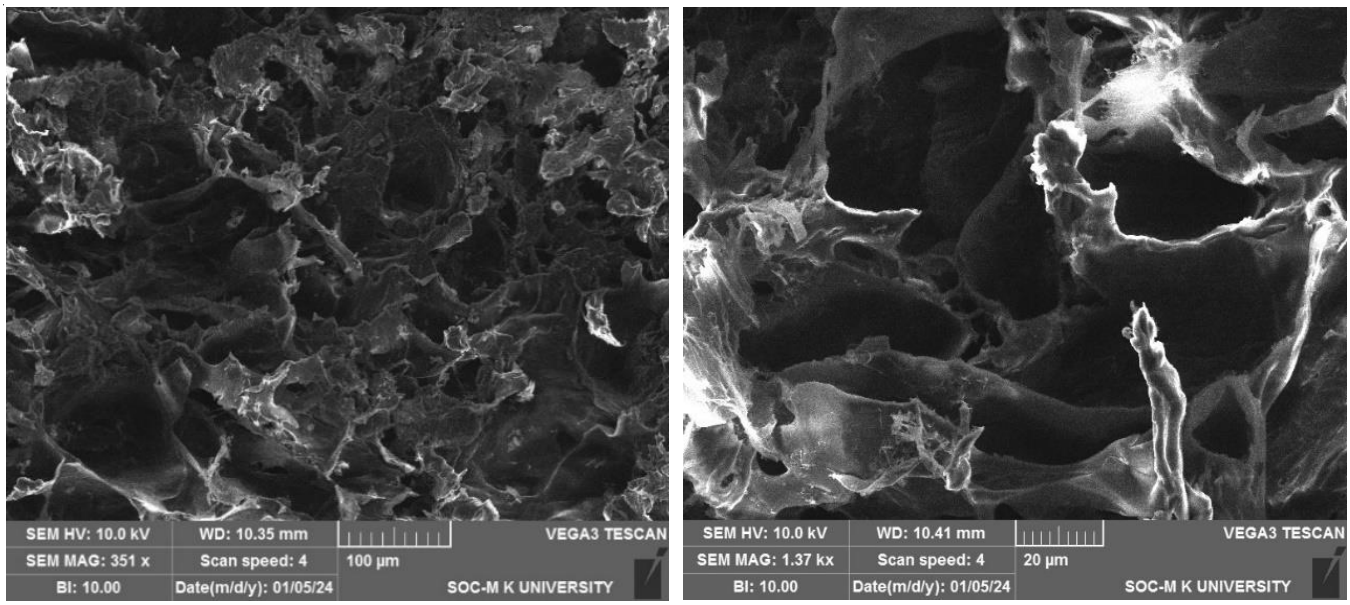

Fig. 6. SEM images of COS-CL-*g*-AM/MBA hydrogel at different magnifications

structure [5]. Therefore, the hydrogel exhibits properties of an efficient adsorbent, making it effective in the removal of Cr(VI) ions.

Adsorption studies: Since adsorption is a reversible process, desorption enables the regeneration and reuse of adsorbent [32]. Consequently, the COS-CL-*g*-AM/MBA hydrogel was used in a batch process for the adsorptive removal of Cr(VI) ions. The adsorption efficiency was evaluated by varying operational factors such as pH, adsorbent dosage, contact time and initial chromium(VI) concentration.

Effect of pH on chromium adsorption: It is well known that pH significantly affects the efficiency of polymeric adsorbents is sorbing heavy metal ions, as it alters both the ionization degree of functional groups and the properties of the metal ions [33]. The pH plays a vital role in regulating sorption by influencing the solubility of metals and the interaction between the adsorbent and the functional groups of hydrogel beads [34,35]. In this study, the pH was varied from 4 to 9. Chromium (VI) adsorption increased from pH 4 to 6 (64%) but then decreased as the pH increased from 7 to 8 (Fig. 7).

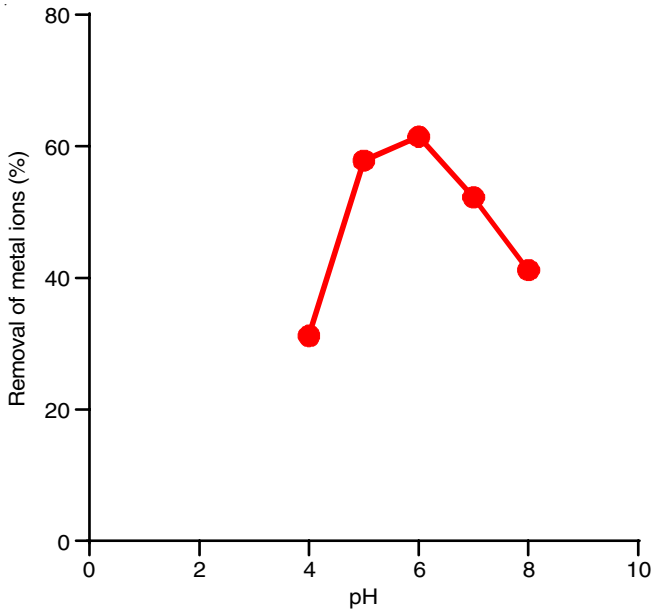

Fig. 7. Effect of pH on chromium(VI) adsorption

Effect of adsorption dosage: Increasing the adsorbent dosage form 1 g to 7 g improved the Cr(VI) removal efficiency up to 6 g, after which equilibrium was reached (Fig. 8). The increased surface area at higher dosages provides more binding sites for the metal ions, enhancing the adsorption allowing more metal ions to be captured [36].

Effect of contact time: An increase in contact time usually results in the improved removal efficiency. Fig. 9 illustrates the percentage of Cr(VI) removal over time. Due to the rapid sorption of metal ions onto the active binding sites, which are more abundant on the external surface of adsorbent, the initial rate of Cr(VI) adsorption was observed to be significantly higher. The quantity of Cr(VI) adsorbed, denoted as q_t, also steadily increased with contact time. However, towards the end of the process, the adsorption and removal rate showed no noticeable change, as the metal ions gradually penetrated the inner pore structures of the adsorbent, leading to the blockage of active binding sites with extended contact duration [37,38].

Effect of initial metal ion concentration: In this study, the initial concentration of Cr(VI) was varied from 25 mg/L to 1000 mg/L to evaluate its effect on adsorption (Fig. 10). At the highest concentration of 1000 mg/L, the metal removal efficiency reached 66.1%. this indicates that the effectiveness of adsorbent in removing Cr(VI) decreases as the initial concentration rises. The observed reduction in removal efficiency may be attributed to the saturation of the sorbent's surface binding sites by Cr(VI), limiting the removal process and lowering the overall removal percentage [8]. Similar results were reported by Badessa *et al.* [39] in their study on Cr(VI) removal from wastewater using powdered banana peel and *Moringa stenopetala* seed powder.

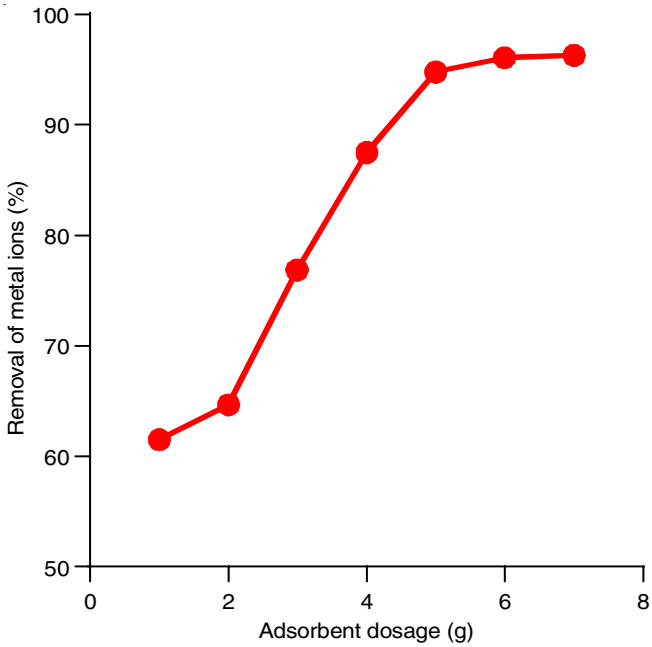

Fig. 8. Effect of adsorbent dosage on chromium(VI) adsorption

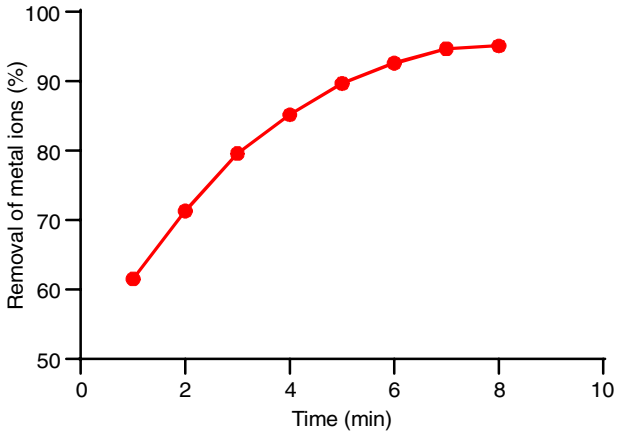

Fig. 9. Effect of contact time on the adsorption of chromium(VI) ions

Adsorption isotherms: To comprehend the interaction between the adsorbent surface and the adsorbed contaminant, it is essential to measure the equilibrium concentration of the adsorbent at each stage of the adsorption process. The adsorption isotherm is defined by the relationship between the equilibrium concentration in the liquid phase (C_e) it interacts with. This curve represents the adsorbent/adsorbate relationship at a constant temperature [40]. Different isotherm models can be used to study the equilibrium behaviour. In this work, the Freundlich and Langmuir isotherm models have been utilized. The Langmuir and Freundlich plots of the Cr(VI) ions are shown in Fig. 11.

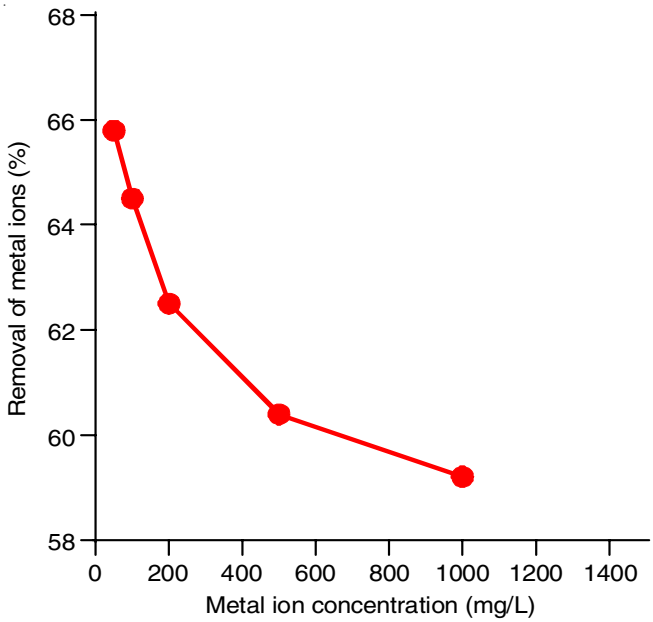

Fig. 10. Effect of initial metal ion concentration of adsorption of Cr(VI) ions

Table-3 indicates that the Langmuir and Freundlich models could more precisely represent the chromium adsorption equilibrium data, as shown by higher R^2 values (*e.g.* 0.9986), with the Freundlich isotherm displaying a higher R^2, suggesting multilayer adsorption. This implies that the adsorption likely follows a predominantly physical adsorption process between the hydrogel and chromium metal, as opposed to a chemical sorption process.

Kinetics of adsorption (COS-CL-*g*-AM/MBA): Kinetic behaviour plays a significant role in the adsorption process,

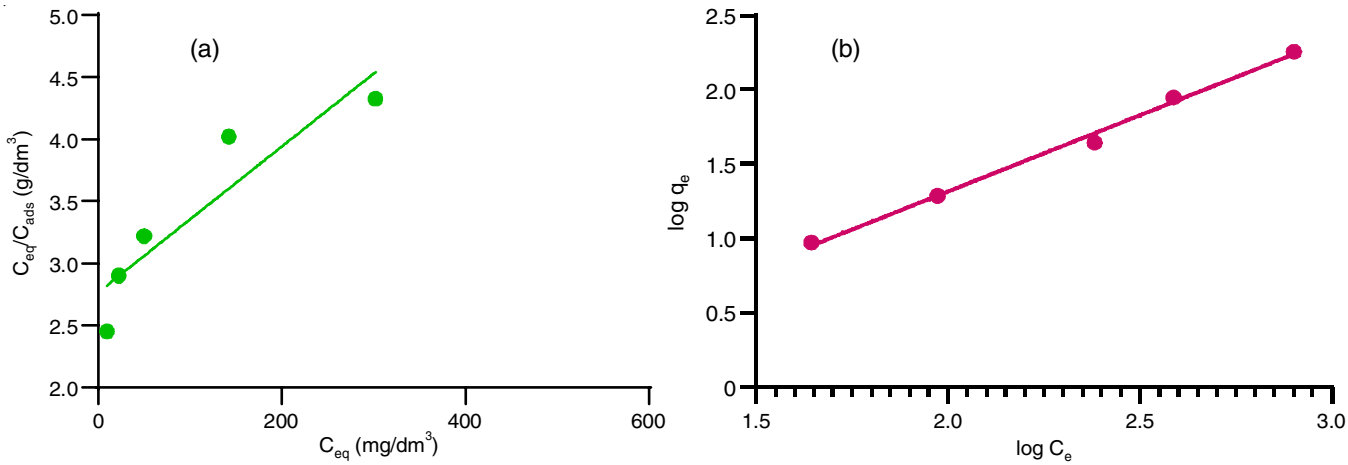

Fig. 11. (a) Langmuir and (b) Freundlich isotherm plots for chromium(VI) adsorption

TABLE-3
LANGMUIR AND FREUNDLICH ISOTHERM CONSTANTS

Metal ions	Langmuir constants				Freundlich constants		
	K_L (dm^3/g)	b	C_{max}	R^2	K_F	n	R^2
Cr(VI)	0.361402	0.002160	193.63	0.841	1.7083	1.255	0.9986

influencing the amount and duration of contaminant adsorption [41]. The rate at which pollutants are adsorbed and equilibrium is established can be used to evaluate the efficiency of an adsorbent in wastewater treatment. The kinetic behaviour of Cr(VI) metal adsorption was studied over a time range of 60 to 420 min using the COS-CL-*g*-AM/MBA adsorbent. The graphs plotting log ($q_e - q_t$) *vs.* t, $1/q_t$ *vs.* t and q_t *vs.* $t^{½}$ are presented in Fig. 12. Table-4 provides a comparison of the theoretical data for the pseudo-first-order and pseudo-second-order and intra-particle diffusion models.

The non-zero value of I and its deviation from the origin suggest that the rate-controlling step in the adsorption process involves mechanisms beyond intra-particle diffusion as shown in Table-4. However, when comparing the correlation coefficients of PFO and PSO, it can be concluded that PSO kinetics govern the adsorption of chromium onto the COS-CL-*g*-AM/MBA hydrogel. The slower bond formation between the metal cation and the active sites of adsorbent, specifically the non-bonded electron pair of nitrogen in the amine groups and the oxygen in the hydroxyl and ester groups is believed to be the rate-limiting step in the adsorption process, as indicated by the dominance of pseudo-second-order kinetics [42].

Mechanism of adsorption: Chromium binds to the hydroxyl surface through ion exchange, electrostatic interactions, dative bonding, hydrogen bonding and van der Waals forces (Fig. 13). As a result, various processes such as physisorption (van der Waals forces, pore-filling) and chemisorption (ion exchange, electrostatic interactions, surface complexation and precipitation) contribute to the efficient uptake of Cr(VI) onto the COS-CL-*g*-AM/MBA hydrogel [43]. Furthermore, the uptake

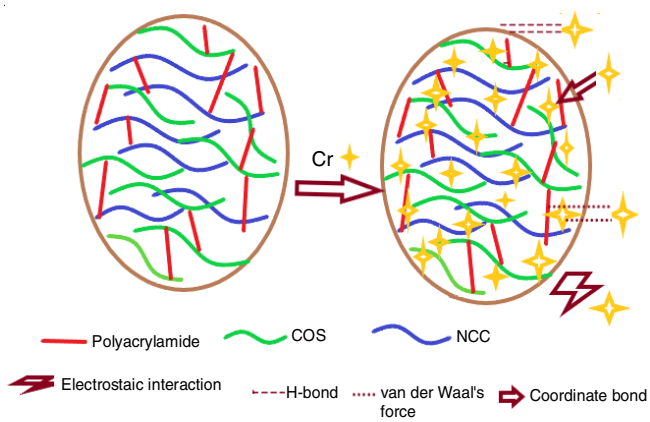

Fig. 13. Mechanism of adsorption of chromium(VI) on COS-CL-*g*-AM/MBA

of metal ions onto the composite can be facilitated by van der Waals forces, film diffusion and intraparticle diffusion [44].

Desorption studies: In this study, the chromium-adsorbed hydrogel underwent desorption trials using two eluting agents, HCl and EDTA, with the results shown in Fig. 14. Among the two, 1 M HCl exhibited a higher chromium removal or recovery efficiency. The percentage of desorption was found to be time-dependent, increasing as the time extended from 1 to 5 h. The process was repeated over three cycles and it was observed that while the desorption percentage decreased slightly with additional cycles, the reduction was not significant. This suggests that the hydrogel remains an effective adsorbent for Cr(VI) removal and recovery over three adsorption-desorption cycles without a major decline in performance [44]. The slight decrease in performance could be due to the saturation of adsorption

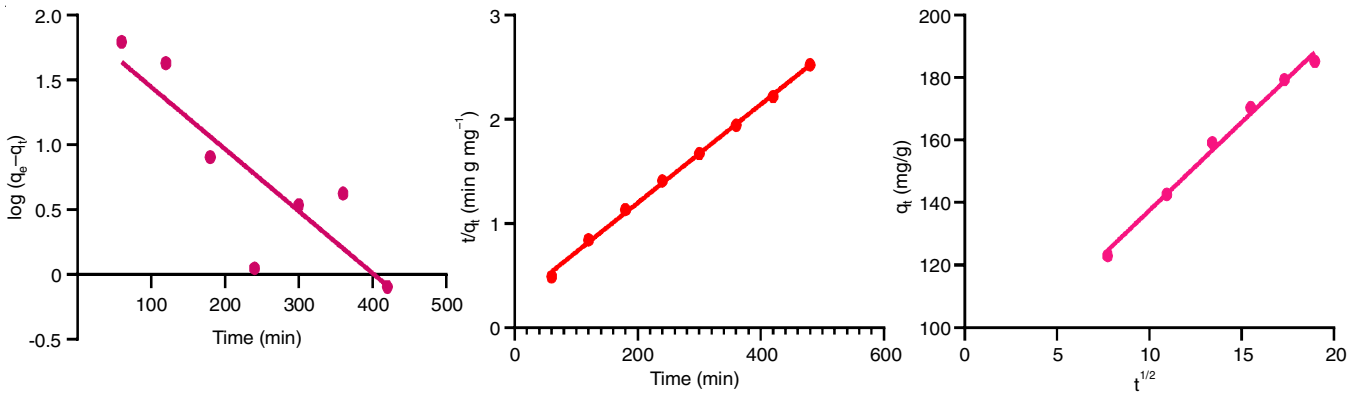

Fig. 12. (a) Pseudo-first order (PFO), (b) pseudo-second order (PSO) and (c) intraparticle diffusion (IPD) kinetic model plots

TABLE-4
PFO, PSO AND IPD KINETIC MODELS

Pseudo-first-order kinetic model			Pseudo-second-order kinetic model			Intra-particle diffusion model		
q_e (mg/g)	k_1 (min^{-1})	R^2	q_e (mg/g)	k_2 (g $mg^{-1}min^{-1}$)	R^2	K_{id}	I	R^2
60.3948	0.0100974	0.7215	211.46	0.000893449	0.9987	1.228	134.8	0.9922

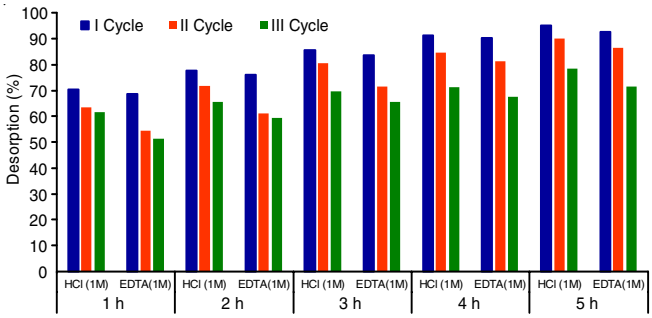

Fig. 14. Desorption of chromium(VI) using EDTA and HCl

sites, changes in the physical and chemical properties of sorbent and possible damage to its microstructure during repeated cycles [45]. The lower efficiency of EDTA compared to HCl may be attributed to its mechanism of metal capture through chelation, whereas HCl removes metals *via* ion exchange. Consequently, after the first desorption cycle, metal adsorption is lower with EDTA than with HCl [46]. When desorbing Cr^{6+} with EDTA, the COS-NCC hydrogel adsorbed with Cr^{6+} was successfully restored. Therefore, adsorbents must exhibit high recycling and recovery capacity [47].

Conclusion

Chitosan oligosaccharide (COS)-based hydrogels present an excellent alternative for sustainable remediation methods due to their attractive characteristics, including hydrophilicity, a rough and porous morphology and a highly functional surface. In this study, the COS/NCC-*g*-AM/MBA hydrogel was synthesized and evaluated using various analytical techniques, demonstrating promising adsorption capabilities. This is supported by XRD, SEM and swelling studies. By modifying several operational parameters such as initial pH and concentration of the metal solution, the quantity of adsorbent used and the duration of agitation between the metal solution and the adsorbent, the hydrogel effectively removed hazardous chromium(VI) ions from the aqueous solutions. The results highlighted that the adsorption process was straightforward and dependent on time and dosage. The sorption process adhered to a physical interaction model, following the Freundlich isotherm and pseudo-second-order kinetics. The desorption studies also confirmed that the recyclability of sorbent, underscoring its cost-effectiveness.

CONFLICT OF INTEREST

The authors declare that there is no conflict of interests regarding the publication of this article.

REFERENCES

1. M. Zhang, L. Song, H. Jiang, S. Li, Y. Shao, J. Yang and J. Li, *J. Mater. Chem. A Mater. Energy Sustain.*, **5**, 3434 (2017); https://doi.org/10.1039/C6TA10513K
2. P.B. Vilela, A. Dalalibera, E.C. Duminelli, V.A. Becegato and A.T. Paulino, *Environ. Sci. Pollut. Res. Int.*, **26**, 28481 (2019); https://doi.org/10.1007/s11356-018-3208-3
3. Y.A. Neolaka, Y. Lawa, J. Naat, A.A. Riwu, H. Darmokoesoemo, B.A. Widyaningrum, Y.E. Lindu, M. Iqbal and H.S. Kusuma, *React. Funct. Polym.*, **166**, 105000 (2021); https://doi.org/10.1016/j.reactfunctpolym.2021.105000
4. G. Zeng, Y. Liu, X. Ma and Y. Fan, *Front. Environ. Sci. Eng.*, **15**, 107 (2021); https://doi.org/10.1007/s11783-021-1395-5
5. H. Li, M. Kruteva, M. Dulle, Z. Wang, K. Mystek, W. Ji, T. Pettersson and L. Wågberg, *ACS Nano*, **16**, 2608 (2022); https://doi.org/10.1021/acsnano.1c09338
6. Z. Wan, M. Li, Q. Zhang, Z. Fan and F. Verpoort, *Environ. Sci. Pollut. Res. Int.*, **25**, 17830 (2018); https://doi.org/10.1007/s11356-018-1941-2
7. S. Lone, D.H. Yoon, H. Lee and I.W. Cheong, *Environ. Sci. Water Res. Technol.*, **5**, 83 (2019); https://doi.org/10.1039/C8EW00678D
8. A. Rekha, K. Vijayalakshmi, A. Alswieleh, P. N. Sudha, J. Rani and A. Vidhya, (2024); https://doi.org/10.1007/s13399-024-05071-3
9. P.S. Prasad, T. Gomathi, P.N. Sudha, M. Deepa, K. Rambabu and F. Banat, *Environ. Technol. Innov.*, **28**, 102741 (2022); https://doi.org/10.1016/j.eti.2022.102741
10. N. Nematidil, M. Sadeghi, S. Nezami and H. Sadeghi, *Carbohydr. Polym.*, **222**, 114971 (2019); https://doi.org/10.1016/j.carbpol.2019.114971
11. S. Sethi, S. Thakur, D. Sharma, G. Singh, N. Sharma, B.S. Kaith and S. Khullar, *React. Funct. Polym.*, **177**, 105318 (2022); https://doi.org/10.1016/j.reactfunctpolym.2022.105318
12. B. Cheng, B. Pei, Z. Wang and Q. Hu, *RSC Advances*, **7**, 42036 (2017); https://doi.org/10.1039/C7RA07104C
13. J. Zhang, L. Wang and A. Wang, *Ind. Eng. Chem. Res.*, **46**, 2497 (2007); https://doi.org/10.1021/ie061385i
14. M.A. Qureshi, N. Nishat, S. Jadoun and M.Z. Ansari, *Carbohydr. Polym. Technol. Appl.*, **1**, 100014 (2020); https://doi.org/10.1016/j.carpta.2020.100014
15. F. Chen, Y. Zhao, H. Zhao, X. Zhou and X. Liu, *Gels*, **10**, 259 (2024); https://doi.org/10.3390/gels10040259
16. Y.H. Teow, L.M. Kam and A.W. Mohammad, *J. Environ. Chem. Eng.*, **6**, 4588 (2018); https://doi.org/10.1016/j.jece.2018.07.010
17. A.B. Linares, J.C. Jiménez, P. López and B.R. de Gáscue, *Orbital: Electron. J. Chem.*, **11**, 71 (2019); https://doi.org/10.17807/orbital.v11i2.1360
18. Q. Yang, X. Pan, K. Clarke and K. Li, *Ind. Eng. Chem. Res.*, **51**, 310 (2012); https://doi.org/10.1021/ie201391e
19. K.K. Mahato, S. Sabbarwal, N. Misra and M. Kumar, *Int. J. Polym. Anal. Charact.*, **25**, 353 (2020); https://doi.org/10.1080/1023666X.2020.1789382
20. R. Shen, H. Wang, K. Wu, J. Gao and J. Li, *J. Appl. Polym. Sci.*, **138**, 50824 (2021); https://doi.org/10.1002/app.50824
21. W.S. Abo-Elseoud, M.L. Hassan, M.W. Sabaa, M. Basha, E.A. Hassan and S.M. Fadel, *Int. J. Biol. Macromol.*, **111**, 604 (2018); https://doi.org/10.1016/j.ijbiomac.2018.01.044
22. S. Han, H. Wang, Z. Sun, H. Zhao and P. Zhang, *Carbohydr. Polym.*, **176**, 135 (2017); https://doi.org/10.1016/j.carbpol.2017.08.066
23. M.K. Yadav, S. Pokhrel and P.N. Yadav, *J. Macromol. Sci. A*, **57**, 703 (2020); https://doi.org/10.1080/10601325.2020.1763809
24. A. Zaharia, A.L. Radu, S. Iancu, A.M. Florea, T. Sandu, I. Minca, V. Fruth-Oprisan, M. Teodorescu, A. Sarbu and T.-V. Iordache, *RSC Adv.*, **8**, 17635 (2018); https://doi.org/10.1039/C8RA01733F
25. S. Pavithra, G. Thandapani, S. Sugashini, P.N. Sudha, H.H. Alkhamis, A.F. Alrefaei and M.H. Almutairi, *Chemosphere*, **271**, 129415 (2021); https://doi.org/10.1016/j.chemosphere.2020.129415
26. A.M. Omer, Z.M. Ziora, T.M. Tamer, R.E. Khalifa, M.A. Hassan, M.S. Mohy-Eldin and M.A.T. Blaskovich, *Molecules*, **26**, 449 (2021); https://doi.org/10.3390/molecules26020449
27. H. Mo and J. Qiu, *Polymers*, **12**, 2672 (2020); https://doi.org/10.3390/polym12112672
28. L. Yue, M. Wang, I.M. Khan, S. Niazi, B. Wang, X. Ma, Z. Wang and W. Xia, *Lebensm. Wiss. Technol.*, **147**, 111663 (2021); https://doi.org/10.1016/j.lwt.2021.111663

29. S. Nara and T. Komiya, *Stärke*, **35**, 407 (1983); https://doi.org/10.1002/star.19830351202
30. E. Radha, T. Gomathi, P.N. Sudha and S. Sashikala, *Polym. Bull.*, **78**, 1109 (2021); https://doi.org/10.1007/s00289-020-03136-0
31. M.A.A. Aljar, S. Rashdan and A. Abd El-Fattah, *Polymers*, **13**, 4000 (2021); https://doi.org/10.3390/polym13224000
32. A.E. Burakov, E.V. Galunin, I.V. Burakova, A.E. Kucherova, S. Agarwal, A.G. Tkachev and V.K. Gupta, *Ecotoxicol. Environ. Saf.*, **148**, 702 (2018); https://doi.org/10.1016/j.ecoenv.2017.11.034
33. C. Jiang, X. Wang, B. Hou, C. Hao, X. Li and J. Wu, *J. Agric. Food Chem.*, **68**, 3050 (2020); https://doi.org/10.1021/acs.jafc.9b07540
34. H. Demey, T. Vincent and E. Guibal, *Chem. Eng. J.*, **332**, 582 (2018); https://doi.org/10.1016/j.cej.2017.09.083
35. F. Naseeruteen, N.S.A. Hamid, F.B.M. Suah, W.S.W. Ngah and F.S. Mehamod, *Int. J. Biol. Macromol.*, **107**, 1270 (2018); https://doi.org/10.1016/j.ijbiomac.2017.09.111
36. S. Rafiaee, M.R. Samani and D. Toghraie, *Synth. Met.*, **265**, 116416 (2020); https://doi.org/10.1016/j.synthmet.2020.116416
37. A.A. Werkneh, N. Habtu and H.D. Beyene, *Am. J. Appl. Chem.*, **2**, 128 (2014).
38. M.K. Rai, G. Shahi, V. Meena, R. Meena, S. Chakraborty, R.S. Singh and B.N. Rai, *Resour. Efficient Technol.*, **2**, S63 (2016); https://doi.org/10.1016/j.reffit.2016.11.011
39. T.S. Badessa, E. Wakuma and A.M. Yimer, *BMC Chem.*, **14**, 71 (2020); https://doi.org/10.1186/s13065-020-00724-z
40. H.N. Tran, *Adsorpt. Sci. Technol.*, **2022**, 5553212 (2022); https://doi.org/10.1155/2022/5553212
41. B. Farasati Far, M.R. Naimi-Jamal, M. Jahanbakhshi, S.A. Khalafvandi, M. Alian and D. Razeghi Jahromi, *J. Mol. Liq.*, **395**, 123839 (2024); https://doi.org/10.1016/j.molliq.2023.123839
42. M.H. Rahaman, M.R. Islam, R. Islam, S.N. Alam, M.S. Rahman, M.A. Rahman and B.A. Begum, *Int. J. Biol. Macromol.*, **257**, 128357 (2024); https://doi.org/10.1016/j.ijbiomac.2023.128357
43. F. Fu and Q. Wang, *J. Environ. Manage.*, **92**, 407 (2011); https://doi.org/10.1016/j.jenvman.2010.11.011
44. R. El-Kaim Billah, M.A. Islam, M.K. Nazal, L. Bahsis, A. Soufiane, Y. Abdellaoui and M. Achak, *Sep. Purif. Technol.*, **334**, 126094 (2024); https://doi.org/10.1016/j.seppur.2023.126094
45. J. Tan, L. Kong, Q. Huang, Y. Gan and S. Lu, *Environ. Res.*, **247**, 118192 (2024); https://doi.org/10.1016/j.envres.2024.118192
46. L. Liu, S. Fan, Z. Wang and J. Hu, *Arab. J. Chem.*, **17**, 105669 (2024); https://doi.org/10.1016/j.arabjc.2024.105669
47. Y. Lu, L. Fan, L.Y. Yang, F. Huang and X.K. Ouyang, *Carbohydr. Polym.*, **229**, 115459 (2020); https://doi.org/10.1016/j.carbpol.2019.115459